Journal of Metals, Materials and Minerals, 35(4), e2376, 2025

Crack development of electroplated NiW alloys and their wettability and tribological properties

Jidsucha DARAYEN[1,2], Suwat PLOYPECH[3], Martin METZNER[4], Claudia Beatriz dos SANTOS[4], Petch JEARANAISILAWONG[5], and Yuttanant BOONYONGMANEERAT[1,*]

[1] *Metallurgy and Materials Science Research Institute, Chulalongkorn University, Bangkok, 10330, Thailand*
[2] *Faculty of Engineering, Thammasat School of Engineering, Thammasat University, Pathum Thani 12120, Thailand*
[3] *Nanoscience and Technology, Graduate School, Chulalongkorn University, Bangkok, 10330, Thailand*
[4] *Fraunhofer Institute for Manufacturing Engineering and Automation, Stuttgart, 70569, Germany*
[5] *Department of Mechanical and Aerospace Engineering, Faculty of Engineering King Mongkut's University of Technology North Bangkok, Bangkok, 10800, Thailand*

***Corresponding author e-mail**: yuttanant.b@chula.ac.th

Received date:
20 April 2025
Revised date:
10 June 2025
Accepted date:
8 July 2025

Keywords:
Ni-W coating;
Cr replacement;
Wear resistance;
Crack density;
Wettability

Abstract

This study investigates how sodium tungstate concentration (20 wt% to 46 wt%) and current density (40 A·dm^{-2} to 60 A·dm^{-2}) affect the microstructure, wettability, mechanical properties, and tribological behavior of electrodeposited Ni-W coatings. Results show that increasing current density markedly raises crack density (from <100 cracks·cm^{-2} to >400 cracks·cm^{-2}), while tungstate concentration has minimal effect. XRD confirms Ni-W solid solution formation, with higher tungsten content refining grains and increasing hardness—peaking at 900 HV at 50 A·dm^{-2} (an 80% rise from 500 HV at 40 A·dm^{-2}). However, excessive stress at 60 A·dm^{-2} leads to microcracking and hardness plateauing (~650 HV to 700 HV). Higher crack density improves wettability (contact angle ~17°), enhancing lubricant retention. Wear tests reveal that coatings with controlled microcrack networks perform better, with wear rates dropping by up to 60% in lubricated conditions. These findings highlight the potential of fine-tuning electroplating conditions to optimize Ni-W coatings as durable, high-performance, and environmentally friendly alternatives to chromium coatings, especially for aerospace, automotive, and industrial applications.

1. Introduction

Hard chrome coatings have long been used in aerospace, automotive, and industrial applications due to their exceptional wear resistance, corrosion protection (with a nickel underlayer), and low friction properties [1-3]. However, their reliance on hexavalent chromium (Cr^{6+}) raises serious environmental and health concerns due to its toxic and carcinogenic nature, prompting stricter regulations, such as the REACH directive in the European Union [4-6]. Consequently, the demand for eco-friendly alternatives has driven extensive research into nickel-based alloys, particularly Ni-W, Ni-Mo, and Ni-P coatings [7,8], which offer comparable mechanical and tribological properties while eliminating hazardous chromium compounds [9-11].

Among these candidates, Ni-W alloys have gained significant attention due to their high hardness, thermal stability, and corrosion resistance. Additionally, the electrodeposition process allows for precise control of composition, grain structure, and mechanical properties, making Ni-W coatings highly tailorable for diverse engineering applications [12,13]. Despite these advantages, one major limitation of conventional Ni-W coatings is their lack of intrinsic surface cracks, which distinguishes them from hard chrome coatings. In chromium coatings, these microcracks serve as lubricant reservoirs, reducing friction and enhancing wear resistance under high-stress applications [12]. However, Ni-W coatings typically exhibit a crack-free surface, limiting their tribological performance.

Several studies have explored strategies to induce controlled surface microcracks in Ni-W coatings to mimic the lubricating effect of chromium coatings. Wang *et al.* [14] demonstrated that increasing current density during electrodeposition could lead to surface crack formation, which improved wear resistance by 23% and 10% under dry and lubricated conditions, respectively, and reduced the friction coefficient by 14% and 5%. Similarly, Eliaz *et al.* [15] reported that microcrack formation in Ni-W coatings could result from hydrogen embrittlement or residual stress [16], which could be mitigated by incorporating iron into the deposit [15,17]. Furthermore, increasing tungsten content in Ni-W coatings has been shown to enhance hardness and tribological performance, but its role in crack formation remains unclear [12,18,19].

Despite these findings, the mechanisms governing microcrack formation in Ni-W coatings and their correlation with tribological performance remain poorly understood. Notably, the combined effects of current density and bath composition on crack development and wear behavior have yet to be systematically investigated. This study aims to bridge these gaps by systematically analyzing how electrodeposition

parameters (current density and sodium tungstate concentration) influence surface crack formation in Ni-W coatings and their impact on friction and wear performance. It is hypothesized that increasing current density beyond a critical threshold will lead to stress accumulation, inducing microcracks that enhance tribological performance by facilitating lubricant retention. Furthermore, the study examines whether Ni-W coatings with controlled crack densities can match or exceed the wear resistance of hard chrome coatings under both dry and lubricated conditions [12,20]. The insights gained from this work will establish a fundamental framework for designing Ni-W coatings with optimized microstructures and tailored tribological properties. By demonstrating a scalable, environmentally friendly alternative to hard chrome, this study contributes to the development of next-generation wear-resistant coatings for aerospace, automotive, and industrial applications.

2. Experimental

2.1 Electroplating process

In the NiW electrodeposition process, each bath component plays a vital role. Nickel sulfate provides nickel ions for the coating matrix, while sodium tungstate supplies tungsten. Tri-sodium citrate acts as a complexing agent, ensuring uniform deposition by stabilizing metal ions. Ammonium chloride improves electrolyte conductivity and pH control. Nine different groups (A-I) of NiW electrodeposits were fabricated using deposition baths (900 mL each) containing specific contents of nickel sulphate (15.8 $g{\cdot}L^{-1}$), tri-sodium citrate (147 $g{\cdot}L^{-1}$), and ammonium chloride (26.7 $g{\cdot}L^{-1}$). Three concentrations of sodium tungstate were explored, namely 15.4 $g{\cdot}L^{-1}$, 46.2 $g{\cdot}L^{-1}$, and 55.4 $g{\cdot}L^{-1}$. The deposition process was carefully controlled, maintaining a constant temperature of 70°C and a stable pH value of 7, adjusted as necessary with H_2SO_4 or NaOH. The electrodeposition setup comprised a steel cathode (2.5 cm × 4 cm) and a platinized anode (5 cm × 8 cm), with 3 cm distance in between. The cathodes were prepared by degreasing in a 60°C NaOH solution for 5 min, followed by etching in a 15% HCl solution for 30 s, and then electro-cleaning in sodium hydroxide at 60°C with a current density of 5 $A{\cdot}dm^{-2}$ for 30 s. After cleaning, the samples were thoroughly rinsed to ensure proper surface preparation for optimal coating adhesion. The current densities of 40 $A{\cdot}dm^{-2}$, 50 $A{\cdot}dm^{-2}$, and 60 $A{\cdot}dm^{-2}$ were applied for 30 min during plating, coupled by bath stirring (200 rpm). The use of high current densities was intentionally chosen to promote the formation of cracks on the NiW surface, as it accelerates deposition and induces residual stresses, which are known to enhance microcrack development in electroplated coatings [14,16]. All the detailed process variables for each sample group are summarized in Table 1.

2.2 Electroplating process

The crack density of the coatings was measured using the line intersect method, where a set of micrographs taken from five distinct areas of the coating surface were overlaid with multiple grid lines. The crack density was then determined by dividing the number of cracks intersecting the lines by the total length of the lines.

To evaluate the wear rate of the NiW coatings under both dry and lubricated conditions, ball-on-disc tests were conducted using a universal mechanical tester (Bruker UMT) equipped with an Al_2O_3 ball (grade 10 cm, 0.5 cm diameter). The wear test specimens were subjected to linear reciprocating motion over a 1 cm wear track, with an applied load of 10 N and a sliding speed of 5 $cm{\cdot}s^{-1}$. The total sliding distance covered was 360 m, completed over a duration of 2 h. The wear volume was analyzed using a laser scanning confocal microscope (Keyence) to assess material loss [21]. Each group of samples was tested three times to ensure consistency. The hardness of the coatings was evaluated using a Vickers microhardness tester, with an applied load of 0.025gF and a dwell time of 10 s. Five measurements were taken at different locations on each sample, and the average hardness value was reported. To investigate the crystal structure and phase composition of the NiW coatings, X-ray diffraction (XRD) analysis was performed using a Bruker D8 Advance diffractometer with Cu-Kα radiation (λ = 1.5406 Å). The XRD scans were recorded in the 2θ range of 20° to 100° at a step size of 0.02°, and phase identification was conducted using the ICDD database.

The wettability of the coatings was assessed using an optical tension meter (Kyowa), where a commercial lubricating oil for shock absorbers was used as the test liquid. Ten different locations on each coating surface were examined, and the average contact angle was calculated. The surface morphology and chemical composition were characterized using a scanning electron microscope (SU3500, Hitachi) equipped with an energy-dispersive X-ray analyzer (X-MaxN, Horiba). Additionally, cross-sectional imaging was conducted to analyze coating thickness and structural integrity.

The combined analyses of crack density, wear resistance, hardness, XRD phase identification, and wettability provide a comprehensive understanding of the mechanical and tribological properties of NiW coatings, ensuring a thorough evaluation of their performance.

Table 1. Process variables of hard chrome NiW electroplating.

Condition	Nickel sulphate ($NiSO_4.6H_2O$) [$g{\cdot}L^{-1}$]	Tri-sodium citrate ($Na_3C_6H_5O_7.2H_2O$) [$g{\cdot}L^{-1}$]	Ammonium chloride (NH_4Cl) [$g{\cdot}L^{-1}$]	Current density [$A{\cdot}dm^{-2}$]	Sodium tungstate ($Na_2WO_4.2H_2O$) [$g{\cdot}L^{-1}$]
A					15.4
B				40	46.2
C					55.4
D					15.4
E	15.8	147	26.7	50	46.2
F					55.4
G					15.4
H				60	46.2
I					55.4

3. Results and discussion

3.1 Surface characterization and crack profile characteristics

The microstructural analysis of Ni-W coatings, as shown in Figure 1, demonstrates significant variations in surface morphology and crack formation depending on the electrodeposition parameters. Coatings deposited at 40 A·dm^{-2} exhibit relatively smooth surfaces with minimal crack formation, whereas those produced at 50 A·dm^{-2} and 60 A·dm^{-2} show a progressive increase in crack density, particularly at higher tungsten concentrations. The crack density rises from 0 cracks·cm^{-1} (Group A) to approximately 400 cracks·cm^{-1} (Group I), indicating a strong correlation between current density and crack formation. This trend aligns with reported values for hard chrome coatings, which typically exhibit crack densities between 150 cracks·cm^{-1} and 400 cracks·cm^{-1}. The observed cracks in Ni-W coatings remain surface-localized and do not penetrate through the coating thickness [15], suggesting they primarily function as stress-relief mechanisms rather than structural defects.

As illustrated in Figure 2, all electrodeposited Ni-W coatings exhibited a thickness range of 12 μm to 16 μm. Variations in sodium tungstate concentration directly affected tungsten incorporation, leading to microstructural changes and modifications in crack morphology. Samples prepared at the same current density (Group A, B, and C) exhibit distinct changes in grain structure and crack distribution as W content increases from 20 wt% (Group A) to 38 wt% (Group B) and 46 wt% (Group C). The microstructure of Group A (low W content) consists of a needle-like morphology with elongated grains, while Group B and Group C (higher W content) transition to a nanostructured nodular morphology, indicative of grain refinement. This transition suggests that W incorporation in the Ni matrix disrupts grain growth and increases residual stress, thereby influencing crack formation.

Further insights from Figure 3 reveal significant variations in surface roughness, crack width, and crack depth across different deposition conditions. The measured crack widths remain consistent at 0.03 μm to 0.04 μm for all samples, but crack depth increases significantly from 0.25 μm (Group A) to 0.8 μm (Group C). The increasing crack depth with W content suggests that higher tungsten incorporation promotes stress accumulation, leading to deeper but still surface-contained cracks[12,22,23]. Unlike hard chrome coatings, which exhibit deep, interconnected cracks, Ni-W coatings maintain shorter, more isolated cracks, likely due to reduced stress intensity and solute atom effects inhibiting crack propagation [12,22].

The formation of cracks in Ni-W coatings is primarily attributed to residual stress accumulation, which arises from a combination of atomic size mismatch between Ni and W and differences in their thermal expansion coefficients [24]. The incorporation of W atoms into the Ni matrix during electrodeposition induces lattice distortions, increasing internal stress within the coating [25,26]. As this stress exceeds the critical threshold, microcracks initiate to relieve stored energy. Additionally, higher current densities promote hydrogen evolution, leading to the entrapment of hydrogen bubbles, which further exacerbates stress accumulation and facilitates crack formation. Figure 3 illustrates this effect clearly in Group I (60 A·dm^{-2}), where a dense crack network and distinct pitting defects associated with hydrogen evolution are observed.

A comparative analysis of coatings deposited at identical sodium tungstate concentrations but varying current densities (Group C, F, and I) further highlights the dominant influence of current density on crack formation [8,27,28]. Crack density increases significantly from 71 cracks·cm^{-1} (Group C at 40 A·dm^{-2}) to 177 cracks·cm^{-1} (Group F at 50 A·dm^{-2}) and 409 cracks·cm^{-1} (Group I at 60 A·dm^{-2}), confirming that current density plays a greater role in crack formation than sodium tungstate concentration. At higher current densities, rapid atomic deposition leads to greater microstructural defect accumulation, exacerbating residual stress and promoting crack development [27,29,30].

These findings establish that current density is the key determinant of crack formation in Ni-W coatings, while sodium tungstate concentration primarily affects grain structure, surface roughness, and crack morphology. This is in line with some limited studies that have shown that higher current densities lead to elevated tensile stress and crack formation in the deposits, and that pulse current deposition could be employed to reduce tensile stress, helping mitigate crack development by enabling stress relaxation and reducing hydrogen incorporation [31,32]. The ability to induce controlled microcracks through optimized electrodeposition conditions and protocols therefore presents a unique strategy for tailoring the tribological performance of Ni-W coatings, particularly for applications requiring enhanced wear resistance, lubricant retention, and mechanical stability.

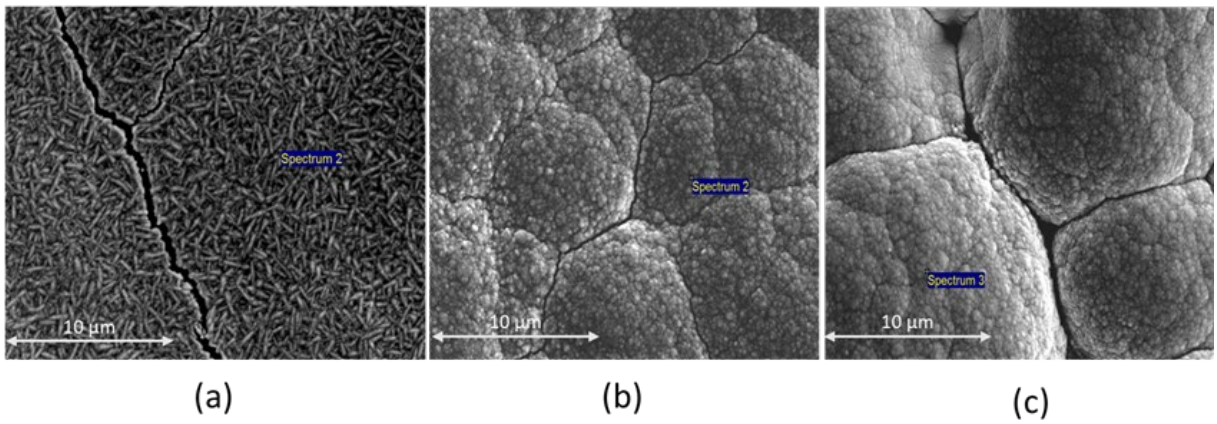

Figure 1. SEM micrographs of samples from Groups (a) (low W), (b) (intermediate W), and (c) (high W).

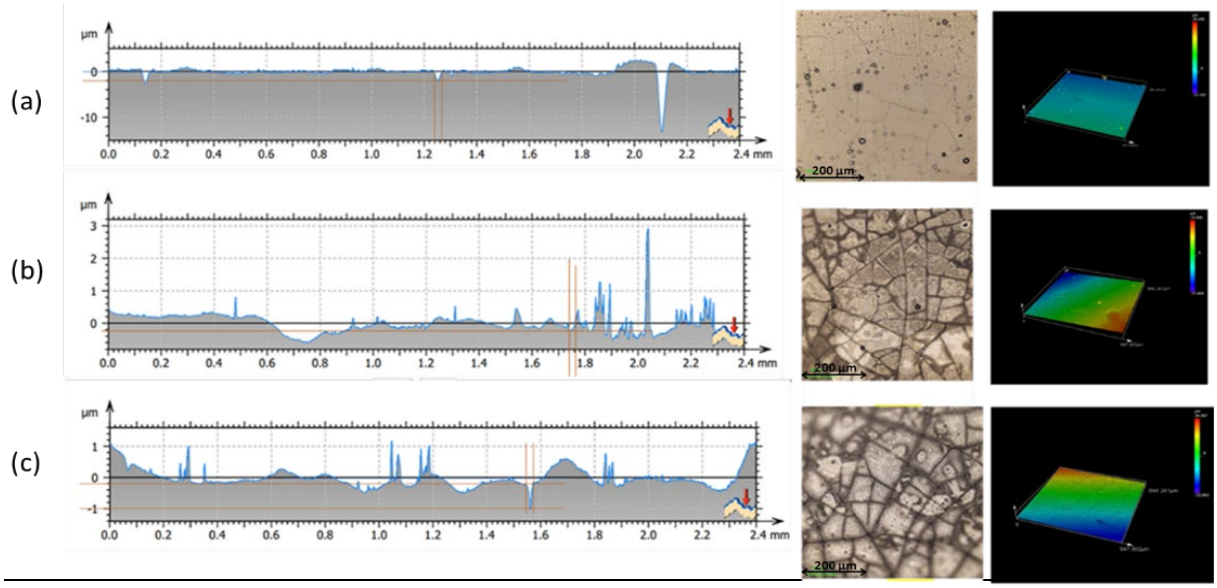

Figure 2. Surface appearance of sample (a) (low W), (b) (intermediate W), and (c) (high W) by varying amount of tungsten which deposited at 40 A·dm^{-2}.

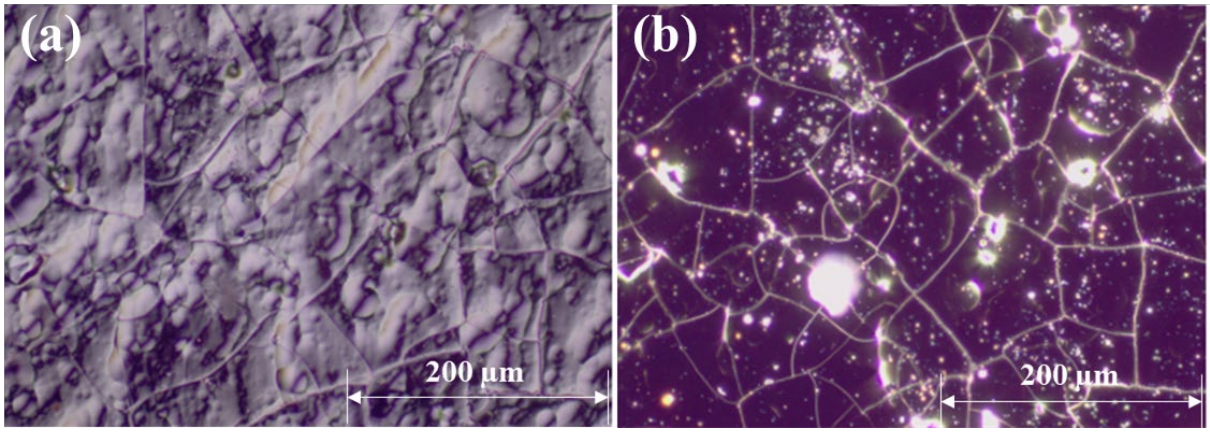

Figure 3. Micrographs of the NiW as-deposited samples from Group I showing (a) surface morphology with crack networks (bright field mode), and (b) defects from hydrogen evolution (dark field mode).

3.2 Wettability

As illustrated in Figure 4, the wettability of Ni-W coatings is strongly correlated with crack density, exhibiting an inverse relationship between contact angle and crack density. The contact angles of all Ni-W samples range from 17° to 36°, indicating a predominantly hydrophilic nature. This is in stark contrast to pure Ni coatings, which typically exhibit a contact angle of ~150°, as reported in previous studies [33]. The substantial reduction in contact angle in Ni-W coatings suggests that microstructural modifications—particularly microcrack formation and surface defects—play a dominant role in altering the wetting behavior. The observed inverse correlation between contact angle and crack density suggests that the presence of microcracks enhances the liquid spreading ability of the coating surface. This effect can be attributed to the capillary action of microcracks, which serve as reservoirs for lubricant retention. As a result, surfaces with higher crack densities (400+ cracks·cm^{-1}, Group I) exhibit the lowest contact angles (~17°), signifying improved lubricant infiltration. Conversely, coatings with lower crack densities (<100 cracks·cm^{-1}, Group A) demonstrate higher contact angles (~36°), indicating reduced wettability.

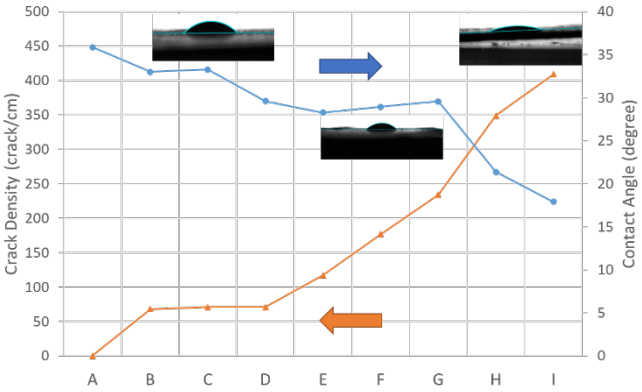

Figure 4. Crack density and the contact angle measurement of the NiW deposits from Group A–I.

Despite the presence of comparable surface roughness across different coating groups, the variation in contact angle can be primarily attributed to microcrack formation rather than topographical effects. The ability of cracks to trap and redistribute lubricant across the contact interface suggests that coatings with high crack densities are more

effective in maintaining lubrication films, thereby contributing to enhanced tribological performance. This finding is particularly significant for applications requiring superior wear resistance under lubricated conditions, where improved wetting behavior can minimize friction and wear losses.

The variation in contact angle across Ni-W electrodeposited coatings may be interpreted using the Cassie–Baxter model, which describes how microstructural features such as roughness, surface voids, and crack morphology influence apparent wettability. According to this model, the apparent contact angle (θ_C) on a heterogeneous rough surface is described by:

$$\cos\theta_C = f_s \cos\theta_Y + (1 - f_s)(-1)$$

where f_s is the solid fraction in contact with the liquid, and θ_Y is the Young's contact angle on a smooth surface. In our study, samples with higher microcrack density and surface roughness—particularly Groups E to G—exhibited significantly lower contact angles (~18° to 25°), as microcracks act as air-retaining features, reducing f_s. This phenomenon leads to a composite wetting state in which water partially rests on air pockets trapped within surface features, lowering the effective contact area and increasing surface hydrophilicity. Similar trends have been reported in prior studies that show enhanced wettability arising from surface textures at micro-scales and nano-scales [34-36]. Moreover, as crack morphology becomes more pronounced, the localized curvature and sharp features enhance air entrapment under the droplet, consistent with theoretical and experimental predictions based on the Cassie–Baxter framework [37,38]. In extreme cases, such as Group G, where microcracks are both deep and wide, partial liquid penetration may occur, shifting the wetting behavior toward a Wenzel-like regime due to increased liquid–solid contact area—a behavior also reported in rough metallic and alloyed surfaces [39,40].

Overall, the results therefore underscore the importance of controlled crack formation in Ni-W coatings, demonstrating that optimized crack densities (~300 cracks·cm^{-1} to 400 cracks·cm^{-1}) provide the most favorable balance between wear resistance and wettability. Excessive cracking, however, may lead to structural weaknesses, emphasizing the need for a precise optimization of electrodeposition parameters to maximize both mechanical durability and tribological performance.

3.3 XRD analysis and its correlation with current density and tungsten content

The X-ray diffraction (XRD) patterns, as presented in Figure 5, confirm the presence of Ni (111), Ni (200), and Ni (220) peaks, along with distinct Ni-W solid solution phases (NiW (111), NiW (200), NiW (220), and NiW (106)), indicating the successful incorporation of tungsten into the Ni matrix [41-43]. As the tungsten content increases from 20 wt% to 46 wt% (Group A to C), noticeable peak shifts and broadening occur, signifying solid solution and grain size reduction, hence enhancement of mechanical strength. At higher tungsten contents (~44 wt% to 46 wt%), Group C, F, and I, the formation of NiW inter-metallic phases becomes more pronounced, further contributing to the observed increase in hardness at moderate to high current densities (40 A·dm^{-2} to 50 A·dm^{-2}).

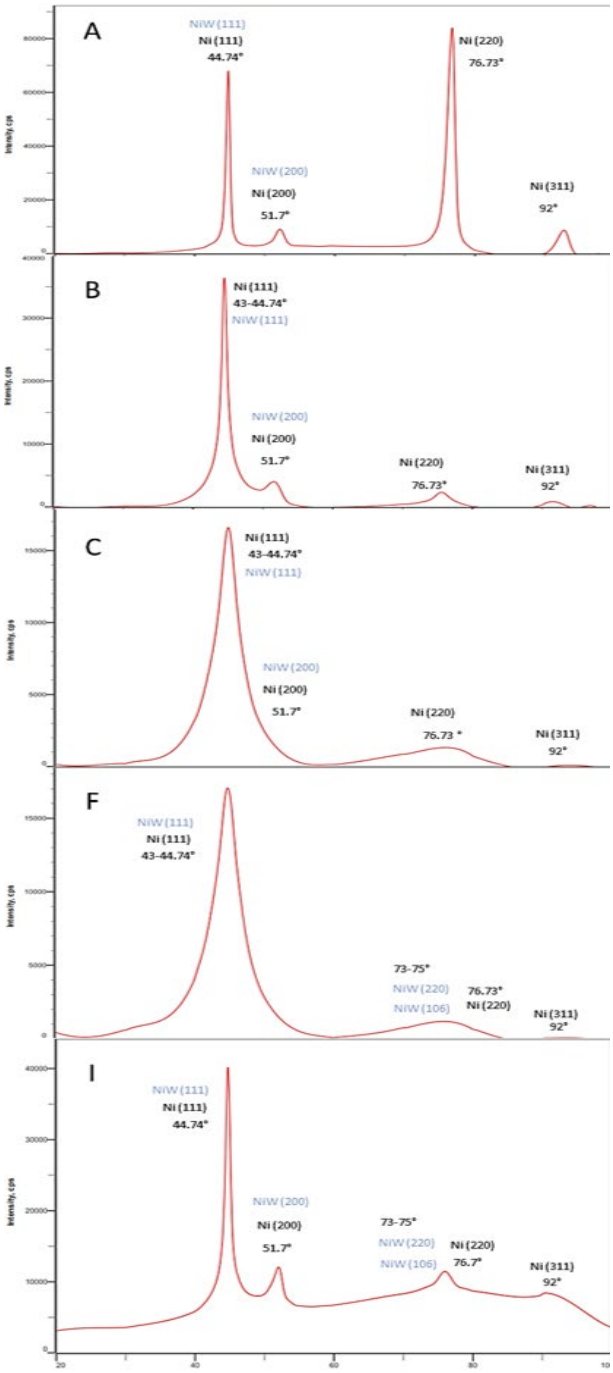

Figure 5. XRD patterns of Ni-W coatings at varying current densities and tungsten concentrations. Peaks correspond to FCC Ni phases (Ni (111), Ni (200), Ni (220)) and NiW solid solutions (NiW (111), NiW (200), NiW (220), NiW (106)). Increased current density enhances W incorporation, with peak broadening in higher-density coatings (e.g., Group I) indicating grain refinement and stress accumulation.

At 60 A·dm^{-2}, the XRD results indicate pronounced peak broadening, particularly in Group G, H, and I, suggesting significant grain refinement due to increased nucleation rates at elevated current densities. This refinement follows the Hall-Petch effect, where smaller grain sizes enhance hardness by increasing grain boundary density, which serves as a barrier to dislocation motion. As a result, coatings deposited at 40 A·dm^{-2} and 50 A·dm^{-2} exhibit progressively higher

hardness values, reaching a maximum of 900 HV at 50 A·dm^{-2} (Group E). However, beyond this threshold, the benefits of grain refinement are counteracted by excessive stress accumulation at grain boundaries, leading to mechanical instability and stress relaxation [12,44,45]. This explains why hardness stabilizes at 60 A·dm^{-2}, where stress relaxation through microcrack formation prevents further strengthening, resulting in hardness values between 650 HV to 700 HV.

These findings demonstrate that the optimal combination of tungsten incorporation and grain refinement occurs at 50 A·dm^{-2}, where solid solution strengthening, Ni-W intermetallic formation, and refined grain structure collectively contribute to maximum hardness. However, at higher current densities (60 A·dm^{-2}), excessive residual stress accumulation and microcrack formation limit further hardness improvements [46,47], emphasizing the importance of precise control over deposition parameters to achieve optimized mechanical properties in Ni-W coatings.

Although sample C, F, and I contain similar W contents (~44 wt% to 46 wt%), their XRD peak profiles differ most likely due to variations in residual stress evolution influenced by current density. Sample I, deposited at the highest current density (60 A·dm^{-2}), exhibits narrower diffraction peaks compared to sample C and F, which is attributed to extensive microcrack formation that acts as a stress-relief mechanism. The release of tensile stress through cracking reduces lattice strain, thereby sharpening the XRD peaks—a phenomenon supported by previous studies on stress relaxation in electrodeposited coatings [48,49]. In contrast, samples C (40 A·dm^{-2}) and F (50 A·dm^{-2}) accumulate higher internal stress without sufficient relaxation, leading to broader peaks associated with greater lattice distortion and smaller crystallite sizes, consistent with structural observations in nanocrystalline Ni-W systems [50].

3.4 Hardness

The hardness of Ni-W coatings was strongly influenced by both current density and tungsten content, as presented in Figure 6. At 40 A·dm^{-2}, the coatings exhibited hardness values ranging from 500 HV to 800 HV, with the highest hardness recorded in Group C (800 HV) [22,51]. This represents a 60% increase compared to Group A (500 HV), attributed to an increase in W content from 20 wt% to 46 wt%. As the current density increased to 50 A·dm^{-2}, the hardness further improved, with Group E reaching 750 HV, marking a 25% increase from Group D (~600 HV) and a significant improvement over Group A. However, at 60 A·dm^{-2}, hardness values stabilized within 650 HV to 700 HV, which is 27.8% lower than Group E but still 30% higher than Group A.

The effect of tungsten content on hardness was particularly significant at 40 A·dm^{-2} and 50 A·dm^{-2}. At 40 A·dm^{-2}, increasing the sodium tungstate concentration from 15.4 g·L^{-1} (Group A) to 55.4 g·L^{-1} (Group C) resulted in a 60% increase in hardness, from 500 HV to 800 HV. Similarly, at 50 A·dm^{-2}, an increase in tungsten content led to an 25% hardness increase, from 600 HV (Group D) to 750 HV (Group E). However, at 60 A·dm^{-2}, despite a high W content (~44 wt% to 46 wt%), the hardness values remained within 650 HV to 700 HV, suggesting a microstructural saturation effect [52,53].

The XRD results provide insights into the structural evolution of Ni-W coatings as a function of current density and tungsten incorporation. At 40 A·dm^{-2} (Group A, B, C), the diffraction patterns show dominant FCC Ni-based peaks (Ni (111), Ni (200), Ni (220)) with moderate tungsten incorporation. As the current density increases to 50 A·dm^{-2} (Group D, E, F), additional NiW solid solution peaks (NiW (111), NiW (200), NiW (220), NiW (106)) emerge, confirming an increase in tungsten content. This structural transformation correlates with the highest recorded hardness (900 HV in Group E), attributed to a combined effect of solid solution strengthening, grain refinement, and increased W incorporation [54,55]. At 60 A·dm^{-2} (Group G, H, I), excessive tungsten incorporation leads to peak broadening, indicating a nanocrystalline structure. While finer grains generally enhance hardness due to the Hall-Petch effect, the observed stabilization of hardness (~650 HV to 700 HV) suggests stress accumulation at grain boundaries, leading to mechanical instability. This phenomenon limits further hardness improvements, as excessive internal stress promotes microcrack formation as a relaxation mechanism.

These findings demonstrate that the optimal balance between mechanical strengthening and stress mitigation occurs at 50 A·dm^{-2} (Group E), where hardness peaks at 900 HV. Beyond this point, excessive tungsten incorporation and structural stress accumulation result in a plateau effect, limiting further hardness enhancement. The correlation between XRD analysis, tungsten incorporation, and microstructural evolution confirms that a precisely optimized current density is essential for maximizing hardness while maintaining coating integrity. These results align with the wear resistance data, reinforcing the role of microstructural engineering in optimizing both mechanical properties and tribological performance of Ni-W coatings.

3.5 Wear resistance of Ni-W coatings

3.5.1 Dry condition

The wear resistance of the Ni-W coatings, as shown in Figure 7(a), demonstrates a significant dependence on both crack density and hardness. The wear rate varies between 2.7 mm^3·cm^{-1} and 5.4 mm^3·cm^{-1}, with a general trend of decreasing wear rate as crack density increases. Group A, with the lowest crack density (~0 cracks·cm^{-1}) and hardness (500 HV), exhibits the highest wear rate of 5.4 mm^3·cm^{-1}, whereas Group I, with a crack density of ~409 cracks·cm^{-1} and a hardness of ~700 HV, shows the lowest wear rate of 2.7 mm^3·cm^{-1}. This trend is consistent with previous studies on hard chrome coatings, which inherently contain surface microcracks that enhance wear resistance [21].

The coefficient of friction (COF) follows a similar trend, ranging from 0.8 in Group A to 0.4 in Group I, reinforcing the role of microcracks in reducing friction and wear loss. The high tungsten content in Group E and Group I (~44 wt% to 46 wt% W) contributes to the coatings' high hardness (900 HV in Group E, 700 HV in Group I), which aligns with Archard's wear law, where wear resistance improves with increasing hardness [56,57]. Additionally, microcracks in the coatings serve as reservoirs for wear debris, preventing excessive abrasive damage to the surface, thereby further reducing material loss [17,21]. The wear rate of hard chrome coatings (crack density: 150 cracks·cm^{-1} to 400 cracks·cm^{-1}) in similar dry conditions ranges between 0.5 mm^3·cm^{-1} to 8 mm^3·cm^{-1}, comparable to the Ni-W coatings studied here [21].

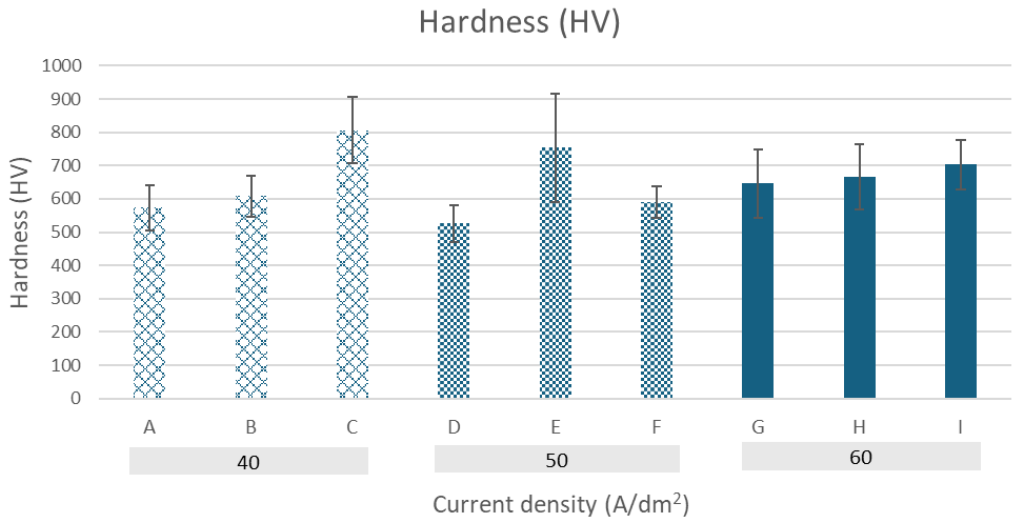

Figure 6. Hardness (HV) of NiW coatings at different current densities and NiW compositions. Maximum hardness (900 HV) is observed at 50 A·dm^{-2} (Group E), while at 60 A·dm^{-2}, hardness stabilizes around 650 HV to 700 HV, indicating saturation. Error bars represent standard.

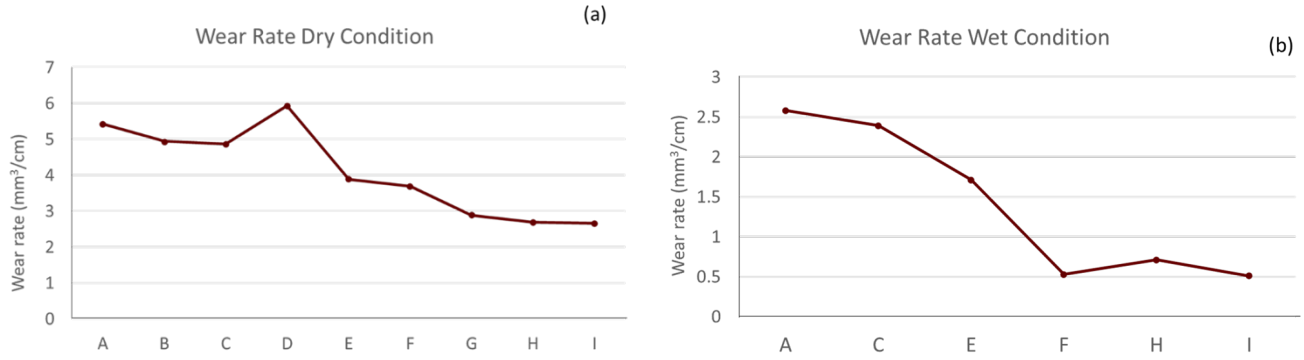

Figure 7. Wear rate (a) in dry condition, and (b) in the lubricated (wet) condition of the NiW samples as a function of crack density.

3.5.2 Wet condition

Under lubricated conditions (Figure 7(b)), the wear rate of the Ni-W coatings is significantly lower than in dry conditions, ranging from 2.6 mm^3·cm^{-1} (Group A) to 0.5 mm^3·cm^{-1} (Group I). The reduction in wear rate is attributed to the formation of a lubricant film, which minimizes direct contact between surfaces and reduces friction. The COF in wet conditions is also lower, remaining between 0.12 and 0.16, further indicating the effectiveness of lubrication. The influence of crack density on wear resistance is more pronounced under wet conditions. The wear rate decreases significantly as crack density increases from 0 cracks·cm^{-1} to 177 cracks·cm^{-1}, reinforcing the idea that microcracks enhance lubricant retention. In Group E and Group I, where crack density is high (~409 cracks·cm^{-1}), the lubricant infiltration into microcracks leads to hydrodynamic lubrication, strengthening the lubrication film and increasing load-bearing capacity [58]. However, beyond 177 cracks·cm^{-1}, the wear rate stabilizes, indicating a limit to the beneficial effect of crack-assisted lubrication.

Interestingly, considering the correlation of surface wettability and wear performance, under the lubricated sliding condition, coatings exhibiting lower contact angles (e.g., Group E, ~18°) demonstrated enhanced oil spreading and retention, which probably facilitated the establishment of hydrodynamic lubrication regimes and resulted in reduced wear rates. In contrast, coatings with higher contact angles (e.g., Group A, ~38°) displayed inferior wetting behavior, leading to limited lubricant coverage and elevated wear. These findings are consistent with studies on textured metallic surfaces, where improved wettability combined with increased surface roughness has been shown to enhance scuffing resistance and lubrication efficiency [59,60]. Furthermore, prior studies have been demonstrated that, under wet conditions, lubrication could fill surface microcracks and thereby blunt crack tips to mitigate crack propagation [61-63]. Conversely, under dry sliding, the absence of lubricant facilitated crack widening and coalescence, accelerating surface degradation. These results align with established tribological principles, which highlight the importance of maintaining continuous lubricant films to prevent debris intrusion and mechanical failure on rough or cracked surfaces.

When compared to hard chrome coatings, which exhibit contact angles of 4.2° to 8.5° and slightly lower wear rates (0.37 mm^3·cm^{-1} to 0.42 mm^3·cm^{-1}) in wet conditions, Ni-W coatings with high crack density (~409 cracks·cm^{-1}) approach similar levels of wear resistance. This suggests that engineered microcracks in Ni-W coatings can provide comparable tribological performance to hard chrome coatings, reinforcing their potential as a viable alternative [12,20]. The XRD analysis supports the observed wear resistance trends, linking the formation of NiW solid solution phases and grain refinement to enhanced mechanical properties. The highest hardness (900 HV in Group E) at 50 A·dm^{-2} is associated with optimized tungsten incorporation and

solid solution strengthening, which contribute to superior wear resistance. However, at 60 A·dm^{-2}, excessive tungsten incorporation leads to stress accumulation and microcrack formation, limiting further improvements in hardness (~650 HV to 700 HV) and wear resistance.

Overall, the results confirm that Ni-W coatings with optimized current density (50 A·dm^{-2}) and controlled microcrack formation offer superior wear resistance, particularly in lubricated conditions where microcracks facilitate lubricant retention. These findings demonstrate that Ni-W coatings can achieve tribological performance comparable to conventional hard chrome coatings, supporting their potential for industrial applications requiring high wear resistance.

The study confirms that current density and tungsten content significantly influence the microstructure, mechanical properties, and tribological performance of Ni-W coatings. Increasing current density from 40 A·dm^{-2} to 60 A·dm^{-2} raised crack density from <100 cracks·cm^{-1} (Group A) to >400 cracks·cm^{-1} (Group I), aligning with XRD findings that indicate NiW solid solution formation and grain refinement at higher W content (~44 wt% to 46 wt%). The highest hardness (900 HV) was achieved in Group E (50 A·dm^{-2}, 55.4 g·L^{-1} W content), marking an 80% increase from Group D (500 HV, 15.4 g·L^{-1} W content). However, at 60 A·dm^{-2}, excessive stress accumulation limited further hardness gains, stabilizing at 650 HV to 700 HV.

Wear resistance improved with hardness and crack density. In dry conditions, the wear rate dropped from 5.4 mm^3·cm^{-1} (Group A, 500 HV, low crack density) to 2.7 mm^3·cm^{-1} (Group I, 700 HV, high crack density), while in wet conditions, it decreased significantly from 2.6 mm^3·cm^{-1} (Group A) to 0.5 mm^3·cm^{-1} (Group I) due to lubricant retention in surface cracks. Contact angle measurements showed an inverse correlation with crack density, where coatings with higher crack densities (~400 cracks·cm^{-1}) exhibited lower contact angles (~17°), enhancing lubrication efficiency.

These findings demonstrate that Ni-W coatings with optimized current density (50 A·dm^{-2}) and controlled crack formation achieve high hardness (900 HV) and superior wear resistance (~0.5 mm^3·cm^{-1} in wet conditions). This suggests that Ni-W coatings are a viable, eco-friendly alternative to hard chrome coatings, offering comparable tribological performance while eliminating hexavalent chromium-related health and environmental risks.

4. Conclusions

This study demonstrates that current density (40 A·dm^{-2} to 60 A·dm^{-2}) and tungsten content (15.4 g·L^{-1} to 55.4 g·L^{-1}) significantly influence the microstructure, hardness, wettability, and wear resistance of Ni-W coatings. Optimal deposition at 50 A·dm^{-2} (Group E) yielded the highest hardness (900 HV), an 80% increase over lower W content coatings. However, at 60 A·dm^{-2}, hardness stabilized (~650 HV to 700 HV) due to stress accumulation and excessive microcracking. Tribological analysis confirmed that coatings with high crack densities (~400 cracks·cm^{-1}, Group I) exhibited superior wear resistance, reducing wear rates from 5.4 mm^3·cm^{-1} (Group A) to 2.7 mm^3·cm^{-1} (Group I) in dry conditions, and from 2.6 mm^3·cm^{-1} to 0.5 mm^3·cm^{-1} in wet conditions. Wettability analysis showed an inverse correlation between crack density and contact angle (~17°), enhancing lubricant retention. These findings establish a framework for engineering Ni-W coatings as a sustainable, high-performance alternative to hard chrome coatings, with potential applications in aerospace, automotive, and industrial wear-resistant components where durability and lubrication efficiency are critical.

Acknowledgements

This research project is supported by the Industrial Postdoctoral Fellowship of Ratchadapiseksompotch Fund Chulalongkorn University. The authors also thanks to the German BMBF for funding the ECOPLATE project under the grant number 01DP17044.

References

[1] H. Kir, and S. Apay, "Effect of hard chrome plating parameters on the wear resistance of low carbon steel," *Materials Testing,* vol. 61, pp. 1082-1086, 2019.

[2] L. Fedrizzi, S. Rossi, F. Bellei, and F. Deflorian, "Wear-corrosion mechanism of hard chromium coatings," *Wear,* vol. 253, pp. 1173-1181, 2002.

[3] M. Mekicha, M. Rooij, D. T. A. Matthews, C. Pelletier, L. Jacobs, and D. J. Schipper, "The effect of hard chrome plating on iron fines formation," *Tribology International,* vol. 142, p. 106003, 2019.

[4] J. Li, C. Yao, Y. Liu, D. Li, B. Zhou, and W. Cai, "The hazardous hexavalent chromium formed on trivalent chromium conversion coating: The origin, influence factors and control measures," *Journal of hazardous materials,* vol. 221-222, pp. 56-61, 2012.

[5] A. Kaparwan, "Hexavalent chromium induced toxicity in nature and living beings," *International Educational Scientific Research Journal* vol. 9, pp. 1-9, 2023.

[6] M. R. Shaibur, "Heavy metals in chrome-tanned shaving of the tannery industry are a potential hazard to the environment of Bangladesh," *Case Studies in Chemical and Environmental Engineering,* vol. 7, p. 100281, 2023.

[7] M. M. Mennucci, R. Montes, A. C. Bastos, A. Monteiro, P. Oliveira, J. Tedim, and M. G. S. Fe, "Nanostructured Black nickel coating as replacement for black Cr(VI) finish," *Applied Sciences,* vol. 11, no. 9, p. 3924, 2021..

[8] M. Arnaudova, E. Lefterova, and R. Rashkov, "Corrosion behavior of electrodeposited nickel-based coatings with W, Mo, and TiOx," *Journal of Solid State Electrochemistry,* vol. 28, no. 5, pp. 1657-1670, 2024.

[9] S. Lu, F. Roudet, A. Montagne, T. Coorevits, G. Guilbert, A. Mouftiez, D. Betrancourt, and D. Chicot, "Vickers hardness of NiW coating as a potential replacement for Cr-VI: A methodology to consider size effect and tip defect in classical microindentation," *Surface and Coatings Technology,* vol. 447, p. 128812, 2022.

[10] M. Srivastava, C. Anandan, and W. V.K, "Ni-Mo-Co ternary alloy as a replacement for hard chrome," *Applied Surface Science,* vol. 285, pp. 167-174, 2013.

[11] P. Trebuňa, D. Kottfer, M. Pekarcikova, A. Petrikova, R. Popovic, F. Rehak, and P. Ciznar, "Evaluating the Replacement of galvanic Cr coatings," *Polish Journal of Environmental Studies,* vol. 27, 2018.

[12] M. H. Allahyarzadeh, M. Aliofkhazraei, A. R. Rezvanian, V. Torabinejad, and A. R. Sabour Rouhaghdam, "Ni-W electro-

deposited coatings: Characterization, properties and applications," *Surface and Coatings Technology,* vol. 307, pp. 978-1010, 2016.

[13] X. Zhang, J. Qin, M. Kumar Das, R. Hao, H. Zhong, A. Thueploy, S Limpanart, Y. Boonyongmaneerat, M. Z. Ma, and R. Liu, "Co-electrodeposition of hard Ni-W/diamond nanocomposite coatings," *Scientific Reports,* vol. 6, no. 1, p. 22285, 2016.

[14] Y. Ko, G. Chang, and J. H. Lee, "Nickel tungsten alloy electroplating for the high wear resistant materials applications," *Solid State Phenomena,* vol. 124-126, pp. 1589-1592, 2007.

[15] N. Eliaz, T. M. Sridhar, and E. Gileadi, "Synthesis and characterization of nickel tungsten alloys by electrodeposition," *Electrochimica Acta,* vol. 50, no. 14, pp. 2893-2904, 2005.

[16] T. J. Rupert, and C. A. Schuh, "Sliding wear of nanocrystalline Ni–W: Structural evolution and the apparent breakdown of Archard scaling," *Acta Materialia,* vol. 58, no. 12, pp. 4137-4148, 2010..

[17] S. Liza, N. Ohtake, H. Akasaka, and J. M. Munoz-Guijosa, "Tribological and thermal stability study of nanoporous amorphous boron carbide films prepared by pulsed plasma chemical vapor deposition," (in eng), *Science and Technology of Advanced Materials,* vol. 16, no. 3, p. 035007, 2015.

[18] M. Donten, "Bulk and surface composition, amorphous structure, and thermocrystallization of electrodeposited alloys of tungsten with iron, nickel, and cobalt," *Journal of Solid State Electrochemistry,* vol. 3, no. 2, pp. 87-96, 1999.

[19] M. Benaicha, M. Allam, A. Dakhouche, and M. Hamla, "Electrodeposition and Characterization of W-rich NiW Alloys from Citrate Electrolyte," *International Journal of Electrochemical Science,* vol. 11, pp. 7605-7620, 2016.

[20] I. Mizushima, P. Tang, H. Hansen, and M. Somers, "Development of a new electroplating process for Ni–W alloy deposits," *Electrochimica Acta,* vol. 51, pp. 888-896, 2005.

[21] S. Ploypech, M. Metzner, C. dos Santos, P. Jearanaisilawong, and Y. Boonyongmaneerat, "Effects of crack density on wettability and mechanical properties of hard chrome coatings," *Transactions of the Indian Institute of Metals,* vol. 72, 2019.

[22] A. J. Detor, and C. A. Schuh, "Tailoring and patterning the grain size of nanocrystalline alloys," *Acta Materialia,* vol. 55, no. 1, pp. 371-379, 2007..

[23] C. N. Panagopoulos, E. P. Georgiou, D. A. Lagaris, and V. Antonakaki, "The effect of nanocrystalline Ni-W coating on the tensile properties of copper," *AIMS Materials Science,* vol. 3, no. 2, pp. 324-338, 2016,.

[24] Y. Xu, D. Wang, M. Sheng, W. Huihua, R. Guo, S. Sheng, and X. Duan, "Study on internal stress of electrodeposition layer of high tungsten Ni-W alloy," *SSRN Electronic Journal,* p. 4243337, 2022.

[25] J. Zhang, P. A. Korzhavyi, and J. He, "First-principles modeling of solute effects on thermal properties of nickel alloys," *Materials Today Communications,* vol. 28, p. 102551, 2021.

[26] G. Dosovitskiy, S. V. Samoilenkov, A. R. Kaul, and D. Rodionov, "Thermal expansion of Ni-W, Ni-Cr, and Ni-Cr-W alloys between room temperature and 800 degrees C," *International Journal of Thermophysics - INT J THERMOPHYS,* vol. 30, pp. 1931-1937, 2009.

[27] Y. Xu, D. Wang, M. Sheng, and H. Wang, "Internal stress of high tungsten content Ni-W alloy coatings," *Surface Engineering,* vol. 39, no. 6, pp. 769-779, 2023.

[28] C.-Y. Hui, T. Liu, and M.-E. Schwaab, "How does surface tension affect energy release rate of cracks loaded in Mode I?," *Extreme Mechanics Letters,* vol. 6, pp. 31-36, 2016.

[29] Y. Boonyongmaneerat, K. Saengkiettiyut, S. Saenapitak, and S. Sangsuk, "Effects of WC addition on structure and hardness of electrodeposited Ni–W," *Surface and Coatings Technology,* vol. 203, no. 23, pp. 3590-3594, 2009.

[30] S. Lee, M. Choi, S. Park, H. Jung, and B. Yoo, "Mechanical properties of electrodeposited Ni-W thinfilms with alternate W-rich and W-poor multilayers," *Electrochimica Acta,* vol. 153, pp. 225-231, 2015.

[31] D. V. Suvorov, G. P. Gololobov, D. Y. Tarabrin, E. V. Slivkin, S. M. Karabanov, and A. Tolstoguzov, "Electrochemical deposition of Ni–W crack-free coatings," *Coatings*, vol. 8, no. 7, p. 8070233, 2018.

[32] K. Ahmadi, S. Brankovic, M. Yarali, and O. Karadavut, *Crack Formation during Electrodeposition and Post-deposition Aging of Thin Film Coatings*. 2019.

[33] R. Zhang, J. Liu, Z. Li, and G. Cui, "A novel superhydrophobic Ni-graphene coating and its corrosion resistance," *Journal of Physics: Conference Series,* vol. 2383, p. 012130, 2022.

[34] K. Kubiak, M. C. T. Wilson, T. Mathia, and P. Carval, "Wettability versus roughness of engineering surfaces," *Wear,* vol. 271, 2011.

[35] M. Razavifar, A. Abdi, E. Nikooee, O. Aghili, and M. Riazi, "Quantifying the impact of surface roughness on contact angle dynamics under varying conditions," *Scientific Reports,* vol. 15, no. 1, p. 16611, 2025.

[36] B. Bhushan, and Y. C. Jung, "Natural and biomimetic artificial surfaces for superhydrophobicity, self-cleaning, low adhesion, and drag reduction," *Progress in Materials Science,* vol. 56, no. 1, pp. 1-108, 2011.

[37] A. Milionis, E. Loth, and I. S. Bayer, "Recent advances in the mechanical durability of superhydrophobic materials," *Advances in Colloid and Interface Science,* vol. 229, pp. 57-79, 2016.

[38] T. L. Liu, and C.-J. C. Kim, "Turning a surface superrepellent even to completely wetting liquids," *Science,* vol. 346, no. 6213, pp. 1096-1100, 2014.

[39] N. Michael, and B. Bhushan, "Hierarchical roughness makes superhydrophobic states stable," *Microelectronic Engineering,* vol. 84, no. 3, pp. 382-386, 2007.

[40] X.-M. Li, D. Reinhoudt, and M. Crego-Calama, "What do we need for a superhydrophobic surface? A review on the recent progress in the preparation of superhydrophobic surfaces," *Chemical Society Reviews,* vol. 36, no. 8, pp. 1350-1368, 2007.

[41] G. Vijaya, M. Singh, M. Krupashankara, and R. S. Kulkarni, "Effect of argon gas flow rate on the optical and mechanical properties of sputtered tungsten thin film coatings," *IOP Conference Series: Materials Science and Engineering,* vol. 149, p. 012075, 2016.

[42] Y. Ma, J. Li, W. Liu, and Y. Shi, "A large-scale fabrication of flower-like submicrometer-sized tungsten whiskers via metal catalysis," *Nanoscale research letters,* vol. 7, p. 325, 2012.

[43] L. Elias, and A. Hegde, "Effect of graphene oxide on the electrocatalytic activity of Ni-W alloy coating," *Insights in Analytical Electrochemistry,* vol. 03, 2018.

[44] L. Yu, J. Cao, and Y. Cheng, "An improvement of the wear and corrosion resistances of AZ31 magnesium alloy by plasma electrolytic oxidation in a silicate–hexametaphosphate electrolyte with the suspension of SiC nanoparticles," *Surface and Coatings Technology,* vol. 276, pp. 266-278, 2015.

[45] C. A. Schuh, T. G. Nieh, and H. Iwasaki, "The effect of solid solution W additions on the mechanical properties of nanocrystalline Ni," *Acta Materialia,* vol. 51, no. 2, pp. 431-443, 2003.

[46] W. Pfeiffer, C. Koplin, E. Reisacher, and J. Wenzel, "Residual Stresses and strength of hard chromium coatings," *Materials Science Forum,* vol. 681, pp. 133-138, 2011.

[47] C. A. Schuh, T. G. Nieh, and T. Yamasaki, "Hall–Petch breakdown manifested in abrasive wear resistance of nanocrystalline nickel," *Scripta Materialia,* vol. 46, no. 10, pp. 735-740, 2002..

[48] J. Sudagar, J. Lian, and W. Sha, "Electroless nickel, alloy, composite and nano coatings – A critical review," *Journal of Alloys and Compounds,* vol. 571, pp. 183-204, 2013.

[49] T. Ziebell, and C. Schuh, "Residual stress in electrodeposited nanocrystalline nickel-tungsten coatings," *Journal of Materials Research,* vol. 27, pp. 1271-1284, 2012.

[50] P. Indyka, E. Beltowska-Lehman, L. Tarkowski, A. Bigos, and E. García-Lecina, "Structure characterization of nanocrystalline Ni–W alloys obtained by electrodeposition," *Journal of Alloys and Compounds,* vol. 590, pp. 75-79, 2014..

[51] K. R. Sriraman, S. Ganesh Sundara Raman, and S. K. Seshadri, "Synthesis and evaluation of hardness and sliding wear resistance of electrodeposited nanocrystalline Ni–W alloys," *Materials Science and Engineering: A,* vol. 418, no. 1, pp. 303-311, 2006.

[52] S. Mbugua Nyambura, M. Kang, J. Zhu, Y. Liu, Y. Zhang, and N. J. Ndiithi, "Synthesis and characterization of Ni–W/Cr_2O_3 nanocomposite coatings using electrochemical deposition technique," *Coatings*, vol. 9, no. 12*,* p. 815, 2019.

[53] T. Wu, M. Ma, K. Ding, X. Nan, Z. Wang, X. Wei, and X. Zhu, "Effect of Y_2O_3 nanoparticles on the microstructure and corrosion resistance of electrodeposited Ni-Mo-Y_2O_3 nanocomposite coatings," *International Journal of Electrochemical Science,* vol. 18, no. 6, p. 100095, 2023.

[54] J. Deng, K. Li, J. Fu, B. Li, H. Jiang, H. Ju, E. Wang, C. Zhang, Y. Liu, Y. Chen, F. Wu, and C. Su, "Preparation and properties of textured Ni–W coatings electrodeposited on the steel surface from a pyrophosphate bath," *Coatings*, vol. 13, no. 9*,* p. 1519, 2023.

[55] N. Sunwang, P. Wangyao, and Y. Boonyongmaneerat, "The effects of heat treatments on hardness and wear resistance in Ni–W alloy coatings," *Surface & Coatings Technology,* vol. 206, pp. 1096-1101, 2011.

[56] S. Park, H. Han, J. Seo, J. Park, S. Yoon, and B. Yoo, "Electrodeposition of nickel-tungsten alloy with functional concentration periodically graded material structure for low stress and high hardness," *Journal of The Electrochemical Society,* vol. 171, 2024.

[57] M. Dadvand, and O. Savadogo, "Effect of pulse reverse current waveform on tribological and mechanical properties of electrodeposited nickel–tungsten alloys on brass substrate," *Tribology - Materials, Surfaces & Interfaces,* vol. 16, no. 4, pp. 281-291, 2022.

[58] K. Tønder, "Hydrodynamic effects of tailored inlet roughnesses: Extended theory," *Tribology International,* vol. 37, pp. 137-142, 2004.

[59] L. Wojciechowski, K. J. Kubiak, and T. G. Mathia, "Roughness and wettability of surfaces in boundary lubricated scuffing wear," *Tribology International,* vol. 93, pp. 593-601, 2016..

[60] C. Zhang, and M. Fujii, "Influence of wettability and mechanical properties on tribological performance of DLC coatings under water lubrication," *Journal of Surface Engineered Materials and Advanced Technology,* vol. 05, pp. 110-123, 2015.

[61] I. Tudela, A. J. Cobley, and Y. Zhang, "Tribological performance of novel nickel-based composite coatings with lubricant particles," *Friction,* vol. 7, no. 2, pp. 169-180, 2019.

[62] Q. Wang, and F. Zhou, "Progress in tribological properties of nano-composite hard coatings under water lubrication," *Lubricants*, vol. 5, no. 1*,* p. 5, 2017.

[63] C. Hu, L. Zhao, Y. Zhang, Z. Du, and Y. Deng, "The influence of hard coatings on fatigue properties of pure titanium by a novel testing method," *Materials*, vol. 17, no. 4*,* p. 835, 2024.